

Journal of Materials Chemistry C

Accepted Manuscript



This is an *Accepted Manuscript*, which has been through the Royal Society of Chemistry peer review process and has been accepted for publication.

Accepted Manuscripts are published online shortly after acceptance, before technical editing, formatting and proof reading. Using this free service, authors can make their results available to the community, in citable form, before we publish the edited article. We will replace this *Accepted Manuscript* with the edited and formatted *Advance Article* as soon as it is available.

You can find more information about *Accepted Manuscripts* in the [Information for Authors](#).

Please note that technical editing may introduce minor changes to the text and/or graphics, which may alter content. The journal's standard [Terms & Conditions](#) and the [Ethical guidelines](#) still apply. In no event shall the Royal Society of Chemistry be held responsible for any errors or omissions in this *Accepted Manuscript* or any consequences arising from the use of any information it contains.

Recent Development in Black Phosphorus Transistors

Haiwei Du[†], Xi Lin[‡], Zhemi Xu, Dewei Chu^{*}

School of Materials Science and Engineering, University of New South Wales, Sydney, NSW, Australia 2052

Abstract

The discovery of graphene has inspired great research interest in two-dimensional (2D) layered nanomaterials during the past decade. As one of the newest members in 2D layered nanomaterials family, black phosphorus (BP), with puckered structure similar to graphene, has shown great potential in novel nanoelectronics owing to its thickness-dependent bandgap. Especially, the unique in-plane anisotropy and high carrier mobility enable BP to be a promising candidate for field-effect transistor (FET) applications. In addition, monolayer or few-layer BP can be combined into van de Waal heterostructures and this opens up a pathway for overcoming existing problems such as impurity scattering and surface degradation or achieving functionalities. In this article, we will review typical physical and chemical properties of BP and provide an overview of the recent development in BP-based transistors. With this review, we also discuss the current challenges in BP transistors and future research directions.

1. Introduction

As a switch in digital circuits, field-effect transistor (FET) is an indispensable building block of most modern electronics. With the minimization of the electronics, one of the urgent issues is to overcome the physical scale limit in silicon-based chips by exploring nanoscale FETs with higher on/off ratios from novel channel materials with sizeable bandgaps (≥ 0.4 eV).¹

In 2004, the emergence of graphene triggered the research on two-dimensional (2D) layered materials with unexpected change in properties when the thickness is reduced down to a single layer or a few atomic layers. Especially, the extremely high mobility originating from massless Dirac feature fermions made graphene to be considered as a hot candidate for FET channel materials.² However, the graphene channel layer cannot be tuned off due to the lack of bandgap,¹ which is essential for FET operation. Alternatively, other 2D layered materials are gaining increasing attention for promising transistor applications as they also possess van der Waals

[†]These authors contributed equally to this work.

^{*}Author to whom correspondence should be addressed, electronic mail: d.chu@unsw.edu.au

interactions between adjacent layers.³ For example, as a typical representative of transition metal dichalcogenides (TMDs), MoS₂ with a relatively large intrinsic bandgap of 1.8 eV shows superior on/off ratio and ultralow standby power dissipation.⁴ Generally, MoS₂ exhibits n-type characteristics because of the presence of S vacancies and strong Fermi-level pinning near the conduction band,⁵ and has great potential in practical electronic and optoelectronic applications.⁶ However, in spite of many promising theoretical predications, the observed mobility of TMDs based device is still relatively low due to the heavy effective mass of carriers and the scattering mechanisms, especially the phonon scattering at room temperature.^{7, 8} Thus, the majority of TMDs materials have not been demonstrated for high-performance radio frequency (RF) transistors.³

At the beginning of 2014, black phosphorus (BP), one of the latest members of 2D layered semiconducting materials has been rediscovered from the perspective of 2D materials for transistors.⁹ Although BP was discovered a century ago, there have been only a few studies focusing on the utilization of BP due to the difficulty in synthesis.¹⁰ Recently, it has been found that the moderate and tunable bandgap of BP provides an alternative for next generation nanoelectronic applications. Similar to graphene, single-layered or few-layered black phosphorus can be obtained by mechanical exfoliation and they exhibit unexpected properties compared with their bulk counterpart. Moreover, as a single-elemental layered material, BP possesses lower spin-orbit coupling because of relatively lighter phosphorus atom, which is more favourable for spin transport.¹¹

The atomic structure and properties of main 2D layered materials are listed in Table 1, in which we select MoS₂ as a representative of TMDs. We also highlight hexagonal boron nitride (h-BN) as a graphite-type structured material, which a good gate insulator for 2D materials based FETs because of its ultra-flat and charged impurity-free surface.¹² According to Table 1 and previous literature,^{13, 14} BP shows many advantages for FET application such as tunable bandgap covering visible to mid-infrared range, relatively higher on/off ratio, intrinsic ambipolar behaviour, lower thermal conductivity and the unique anisotropy. In particular, this unique anisotropy can be utilized for developing novel thermoelectric, photonic and optoelectronic devices.

In this review, we aim to underscore the recent progress in BP transistors and their potential applications. In section 2 the structure and fundamental properties including electrical, thermoelectric, optical and mechanical properties are presented. Section 3 presents the development of BP transistors and current challenges. In section 4, we aim to introduce BP based heterostructures for novel functionalities. Finally, in section 5 the conclusion remarks and outlook are presented.

2. Structure and Fundamental Properties

A century ago, BP was synthesized from white phosphorus and the required phase transformation condition from white phosphorus to BP was under 1200 MPa, 473 K.³² Although BP is the most stable member of phosphorus family, it can still react with oxygen and water molecules, and the rapid surface oxidation affects the contact resistance, carrier mobility, as well as the hysteretic behaviour in I_{ds} - V_{bg} characteristics.³³ The synthesis details of BP have been summarized by Ye's group recently and a comprehensive review of BP is beyond the scope of this article.²² Here, we focus on the fundamental properties including crystal structure, electrical, optical and mechanical properties.

2.1 Structural Characteristics

Similar to graphite, bulk BP consists of layered hexagonal honeycombs and the single layer of BP also can be obtained by mechanical exfoliation. Under normal conditions, BP structure is orthorhombic with space group *Cmca*. Under high pressure, a phase transition was found, exhibiting a transformation from orthorhombic to rhombohedral structure at ~5 GPa and further to simple cubic structure at ~10 GPa.³⁴ Fig. 1a shows the atomic structure of BP. Each atom is bonded to three neighbouring atoms and this honeycomb puckered network is formed by sp^3 hybridization between phosphorus atoms since phosphorus element has only three valence electrons. Similar to the naming of graphene, the monolayer or few-layer BP is named as phosphorene, as shown in Fig. 1b. The individual layers of phosphorus atoms are held together by weak van der Waals forces and van der Waals interactions are dominant along the crystallographic y direction.³⁵ It is seen that the single-layer consists two atomic layers, in which the bond distance between the nearest atoms d_1 is 2.224 Å and the length of connection between top and bottom atoms d_2 in the single-layer is 2.244 Å.³⁶ The values of d_1 and d_2 are very close and this is ascribed to the covalent bonds derived from phosphorus 3p orbitals.³⁶ In addition, several new phosphorene polymorphs with buckled honeycomb structure or non-honeycomb structure were predicted by computational studies, enriching the phosphorene family with variable members.³⁷⁻³⁹ The x and y directions in BP structure correspond to the armchair (AM) and zigzag (ZZ) direction respectively, and it should be noted that the in-plane anisotropy resulting from these two directions is very unique. For example, a high degree of anisotropy of effective masses has not been found in other 2D materials.⁴⁰

2.2 Fundamental Properties

In this section, the electrical, thermoelectric, optical and mechanical properties will be introduced. Before this part, it is noted that the most unique property of BP is its strong in-plane anisotropy arising from the atomic structure. Herein, we will briefly focus on the anisotropy in electronic transport and thermal conduction.

2.2.1 Electrical Properties

Similar to dichalcogenides, the bandgap of BP shows thickness dependence, increasing from ~ 0.3 eV for bulk to ~ 2 eV for monolayer,^{9, 19, 23} which is attributed to the interlayer interactions with the increasing layer numbers. The semiconducting dichalcogenides only have indirect bandgap in multilayers,⁴¹ while the bandgap of BP is direct for all thicknesses.

Because of the intrinsic ambipolar behaviour, BP is quite suitable for complementary metal oxide semiconductor (CMOS) applications. However, it should be noted that the conduction type in BP is hole-dominated transport and it probably can be ascribed to two reasons. The first one is that the activation energy for p-type black phosphorus is lower than that of n-type.²² The second one is the higher degree of anisotropy of the hole effective mass.⁴⁰ Compared with thinner films, a relatively thicker BP flake is favourable for improving ambipolar transport characteristic since the Schottky barrier height for the electron injection is lower. Moreover, a recent computational study reported that introducing electron density (n_{2D}) above $1.3 \times 10^{14} \text{ cm}^{-2}$ could lead to the presence of superconductivity, of which critical temperature (T_C) is above liquid-helium temperature when $n_{2D} > 2.6 \times 10^{14} \text{ cm}^{-2}$.⁴²

Anisotropic electronic transport: Distinct anisotropy was found in charge transport. Ji *et al.* reported that the hole mobility along y direction of monolayer BP is 16-38 times larger than that of along x direction, and they attributed it to the higher elastic modulus along y direction as relatively stiffer 2D materials exhibit higher carrier mobility.⁴³ Moreover, previous observation of anisotropic excitons in quasi-one-dimensional materials has been experimentally reported in 2D monolayer BP,⁴⁴ and the strong anisotropic 2D electron gas (2DEG) in monolayer BP resulted in quantum Hall effect very recently.⁴⁵

It is known that BP not only exhibits strong anisotropy but also shows layer-tunable and strain-dependent electrical properties. As a member of van de Waal materials family, its physical properties always depend on the number of stacked layers to some extent. In addition to the thickness impact on bandgap and mobility,^{19, 23} modification of BP layers can be utilized for improving device performances. Das *et al.* experimentally confirmed the effect of flake thickness on phosphorene transistor, in which the on/off ratio decreases with the increasing layer number because of the reduced Schottky barrier heights for both holes and electrons.⁴⁶ A computational work also showed that the work function decreases monotonously with the increasing layers, which is a practical way to tune Schottky barrier for efficient carrier injection.⁴⁷

Notably, as an important external stimulus, strain shows significant influence on the electronic properties such as gap modification,⁴⁸ direct-indirect bandgap transition,²³ semiconductor to metal transition,⁴⁹ electron-phonon coupling enhancement,⁵⁰ and superconductivity.⁴² The strain effect on phosphorene will not be introduced in detail as it has been summarized in a recent review article.⁵¹ Furthermore, Yakobson *et al.* found that the in-plane anisotropy of phosphorene can be further enhanced by applying directed uniaxial stress which breaks the symmetry.⁵² For example, the bandgap increases monotonically when the stress direction is changed from ZZ to AM.

2.2.2 Thermoelectric Properties

Since heat generation inevitably exists in electronic devices, using thermoelectric materials as the FET channel can not only efficiently convert the waste dissipation heat to electrical energy but also protect the device in case of performance degradation and breakdown, providing a new route to realize high efficient chip-cooling. Thermoelectric property is to establish a direct conversion between thermal and electrical energy and it shows great potential for solving future energy and environmental issues. In order to achieve high conversion efficiency, high electrical conductivity and low thermal conductivity are required simultaneously. With much lower thermal conductivity than graphene (as shown in Table 1), BP has been considered as a promising candidate for novel thermoelectric applications.²⁸

Anisotropic thermal conduction: It is well-known that the thermal transport of 2D materials is mainly determined by phonon-phonon scattering.⁵³ Fig. 2 shows the calculated thermal conductivity of BP from previous work,⁵⁴⁻⁵⁷ and it is found that thermal conductivity along the ZZ direction is much larger than that along the AM direction either in phosphorene or bulk BP. This anisotropy in thermal conductivity is attributed to the orientation-dependent group velocities resulting from anisotropic phonon dispersion, as the group velocities along the ZZ direction are much larger than those along the AM direction.^{54, 55, 58} A strong orientation-dependent shear modulus is also an indicator for this strong anisotropy of phonons transport.⁵⁹

Unlike anisotropic electrical conduction and thermal transport, Seebeck coefficient is almost isotropic.^{58, 60-62} Electrical and thermal transport exhibit respectively orthogonal preferred conducting directions, and a large electrical conductivity/thermal conductivity ratio for thermoelectric application can be achieved, as shown in Fig. 3a.⁶¹ From Fig. 3d and e, the figure of merit ZT value is larger along armchair direction than that of zigzag direction, indicating a strong anisotropy. Notably, a series of research theoretically demonstrated that a huge ZT value can be achieved in BP with optimized conditions and modulated by strain engineering.⁶¹⁻⁶⁴

Based on the predictions, thermoelectric properties of BP were evaluated indirectly by measuring photocurrent response at first.^{65, 66} Pan *et al.* demonstrated that the generated electron-hole pairs after light absorption contribute to photocurrent, which is attributed to the voltage difference resulting from the Seebeck coefficient difference between the BP and electrode.⁶⁵ Low *et al.* demonstrated that the observed photocurrent polarities and dependencies are dominated by thermally driven thermoelectric and bolometric processes rather than photovoltaic effect.⁶⁶ Moreover, direct measurement of thermoelectric properties expectedly was reported very recently.⁶⁷ With the natural p-type doping, the Seebeck coefficient increases with increasing temperature, which is attributed to the increase of hole mobility. The articles focusing on thermoelectric properties were summarized in Table 2.

2.2.3 Optical Properties

Interlayer coupling plays a critical role in layered materials and it can be directly reflected by low-frequency breathing modes and shear modes of Raman spectra.⁶⁸⁻⁷⁰ For example, with different thicknesses, anisotropic effect of the interlayer coupling has been demonstrated because of a strong orientation-dependence of the lattice constant.⁵⁹ Moreover, as the thickness increases, large interlayer force constant originating from the sizable covalent interaction between phosphorus atoms in adjacent layers has been confirmed, because the breathing modes have a large red shift in frequency.⁷⁰

2.2.4 Mechanical Properties

The mechanical properties of black phosphorus also have been investigated in the past few years. It has been found that 2D phosphorene shows sensitive electronic structure under strain, superior mechanical flexibility, highly anisotropic and nonlinear mechanical properties. It is believed that the strain can be utilized to modulate the electronic properties of 2D materials, while recent studies have indicated that by applying appropriate axial strain, 2D BP layered materials can even exhibit a switching from direct to indirect band gap transition⁴⁸ and the changing preference of charge transport.⁷¹ Furthermore, Peng *et al.* have demonstrated that phosphorene can sustain a tensile strain up to 30%, which is better than the tensile strain limits of graphene and molybdenum disulphide.^{72, 73} Because of the unique puckered structure, a negative Poisson's ratio traditionally observed in auxetic materials has been found in 2D phosphorene.⁷⁴ In addition, the Young's modulus indicates that single-layer BP has strongly anisotropic mechanical properties because the *x*-direction is more ductile than the *y*-direction.⁶⁴ In comparison to other 2D materials such as graphene and MoS₂, single-layer BP also exhibits excellent flexibility because of the smaller Young's modulus.⁷⁵ The mechanical properties of BP have been applied in nanoelectromechanical systems and the device shows promising nanoelectromechanical attributes.⁷⁶

3. BP Transistors

BP has several advantages for FET applications, as followings:

(i) The tunable bandgap and comparable mobility satisfy the FET requirement, and superior performance such as relatively higher on/off ratio and fast operation are expected because of lower off current resulting from sizable bandgap. The lower direct current power dissipation is also beneficial for offering lower power and higher power efficiency.⁷⁷

(ii) BP shows a distinctive characteristic which is the ambipolar behaviour. It is known that both n- and p-type transport are required in CMOS logic circuits. Since the band structure calculation showed that effective masses of the conduction and the valence band do not differ very much,⁹ the p-type behaviour can be switched to n-type transport by controlling the channel length, back gate voltages, and drain biases.⁷⁸ This unique ambipolar characteristic indicates that BP is very promising for CMOS applications.

(iii) Compared with other 2D semiconductors, the unique anisotropy of charge transport makes contribution to considerable performance improvements in BP, and the monolayer BP transistor shows higher ON-current and faster switching speed than that of MoS₂ transistor.⁷⁹

(iv) As a new member of 2D crystalline nanomaterials family, BP inherits the common properties, including high elasticity and superior flexibility. Therefore, BP based transistors show great potential for future flexible electronics and they are also expected to be compatible with previous 2D materials because of the common van der Waal interaction among layered structure.

A schematic configuration of a typical BP FET device is shown in Fig. 4. According to previous studies,^{9,78,80-82} heavily doped silicon is used as the gate electrode and back-gated configuration is preferentially selected. The gate insulators selections are ranging from conventional SiO₂ to novel 2D insulator, for example hexagonal boron nitride. Meanwhile, with higher work function, Au/Ti was commonly used as the S/D electrodes especially for optimizing hole transport because of the reduced hole injection barrier to the valence band.

3.1 Field-effect transistors

In 2014, a study conducted by Chen *et al.* and Zhang *et al.* attracted much attention and spurred wide-spread scientific research in exploring novel 2D semiconductor black phosphorus transistors with ambipolar behaviour.⁹ The drain current modulation (10^5) at room temperature is four orders of magnitude larger than that in graphene and the large mobility ($\sim 1,000 \text{ cm}^2 \text{ V}^{-1} \text{ s}^{-1}$) is superior to that of commercial silicon-based devices. They also pointed out that the existing lower on-state current and higher subthreshold swing (SS) could be

improved by optimizing gate insulators in the future work. After this innovative study, the effects of anisotropy and thickness on the device performances were successively investigated.^{14, 46} In addition, theoretical investigations^{40, 83, 84} and practical applications^{80, 85} have been reported.

It is known that the anisotropy plays a critical role in charge transport of black phosphorus. Theoretical study based on density function theory shows that the current characteristics are transport direction dependent,⁴⁰ in which the lower effective masses along the armchair direction and higher degree of anisotropy are beneficial to higher drive current in p-type conduction. Other work by the non-equilibrium Green's function formalism (NEGF) also demonstrated the device performances substantially depend on the transport direction, and this unique highly anisotropy is especially favourable for improving the on-state current of transistors with the channel length below 10 nm.^{79, 83, 84}

On the other hand, BP transistors exhibit great potential for ultra-high frequency operation and broadband optical devices. Xia *et al.* first reported the gigahertz frequency operation of BP, exhibiting a peak short-circuit current gain cutoff frequency f_T of 12 GHz and a maximum oscillation frequency f_{max} of 20 GHz, which indicates BP is a promising candidate for power and voltage amplifiers operating in multi-GHz frequency range.⁸⁵ Since BP exhibits layer-tunable bandgap and the transistor can be operated in the near-infrared (NIR) part of the spectrum with a fast photo-response, it is expected that BP can be used for broadband high-speed optical devices such as photodetector and optical switcher.^{80, 86, 87}

Another important feature is focusing on flexible device applications. 2D layered semiconductor materials have been considered promisingly for future flexible electronics because of superior elasticity, bendability and thickness scalability when they are scaled down to monolayer or a few layers. BP is also considered suitably for high-speed electronics and digital circuits on flexible substrates. For example, flexible BP devices on polyimide substrate have been fabricated recently, and the current modulation still showed a maintainable value of 10^3 after applying tensile strain loading (2% uniaxial strain) and multi-cycle bending (5,000 bending cycles).⁷⁷ Compared with other MoS₂ based flexible transistors, the maximum hole mobility ($310 \text{ cm}^2 \text{ V}^{-1} \text{ s}^{-1}$) and electron mobility ($\sim 89 \text{ cm}^2 \text{ V}^{-1} \text{ s}^{-1}$) of BP transistor showed fivefold and triple increase respectively. Furthermore, they designed the inverting and non-inverting configurations simultaneously in a same BP transistor, and a highest circuit amplification factor (voltage gain of 8.7) among reported BP transistors was achieved.

Recent work on BP transistors was summarized in Table 3 and we also can see the hole-transport-dominated characteristic in BP transistors. In spite of the intrinsic superior properties, the remaining challenges are that BP transistors still suffer from some drawbacks including hole-transport-dominated ambipolar characteristics,

Schottky barrier and surface degradation. Relevant investigations focusing on these issues have been reported and will be introduced in the following part.

3.1.1 Balancing ambipolar behaviour

In CMOS circuits, ambipolar channel materials with symmetric n- and p-type behaviour are preferentially selected since they can effectively simplify circuit design and save layout area.⁹⁹ Although BP transistors possess intrinsic ambipolar characteristics, it is found that BP exhibits a strong asymmetric ambipolar behaviour because of the existed high charge (electron) trapping sites on the surface. As a result, the concentration and mobility of electrons are lower than that of holes due to the trapped charge scattering, which is unfavourable for complementary logic devices. As shown in Table 3, the recent studies mainly focused on hole transport. In order to meet the requirements of CMOS applications, it is necessary to modulate p- or n-type doping level. Based on the work function theory, decorating other materials with lower work function can reduce the BP work function and provide sufficient electron to fill the charge trap sites, fulfilling electron transfer to BP.

Recently, Cs₂CO₃ and MoO₃ were used to act as work function modifier to tune the doping level and enhance the performance.⁸⁸ With surface deposition of 10 nm Cs₂CO₃, the electron mobility was remarkably increased by ~25 times from 1 cm² V⁻¹ s⁻¹ to 27.1 cm² V⁻¹ s⁻¹ (as shown in Fig. 5a), indicating the effective enhancement of electron transport. From Fig. 5b, we can even see the presence of electron-transport-dominated characteristic, and this phenomenon is attributed to the work function difference between Cs₂CO₃ and BP. With lower work function than BP, modification of Cs₂CO₃ shows reduced work function with increasing Cs₂CO₃ thickness, followed by decreased contact resistance, originating from substantial interfacial electron transfer from Cs₂CO₃ to BP. As a result, the Fermi level was shifted closer to conduction band. While MoO₃-modified BP further enhance the hole-transport-dominated ambipolar due to higher work function. The variation of work function was also measured by *in situ* ultraviolet photoelectron spectroscopy (UPS) and X-ray photoelectron spectroscopy (XPS) analysis, as shown in Fig. 5c and d.

Unlike the usual back-gated configuration, a top-gate configuration with n-type-dominated transport has been constructed very recently and the results showed that the tuning of carrier type was sensitive to the position of dielectric layers and the deposition conditions.⁸⁷ On the other hand, Schottky barrier heights for electron injection are lower in thicker flakes, resulting in smaller $I_{\text{hole}}/I_{\text{electron}}$ ratio.⁴⁶ Therefore, optimizing device structure, fabrication conditions as well as flake thickness should be studied in the future.

3.1.2 Modulating Schottky barrier by electrode design

It is well-known that the charge carrier conduction is affected by the difference of work function between metal electrodes and semiconductors. Electrodes with higher work function often leads to the presence of Schottky barrier and it has a negative effect on electron transport in field-effect transistors due to forming a depletion region at the interface to prevent the electrons flow into the semiconductor channel layer. This phenomenon was also observed in BP transistors due to the contact metals with high work function⁹ and the oxidation of BP in contact regions.^{23, 65} For example, Schottky barrier height $\Phi_b \approx 0.21$ eV for holes at the Ti/phosphorene interface was measured,²³ and the reduced mobility was a result of a large contact resistance in the source/drain regions. Generally, selecting metal with proper work function is an effective and common solution to minimize the Schottky barrier height and optimize the device performances. Based on the *ab initio* calculations, Zhang *et al.* predicted that an excellent Ohmic contact can be formed at Cu/BP junction while other metals including Zn, In, TaP and NbP will form Schottky contacts where the electronic potential barrier increases with the averaged distance between monolayer BP and metal.¹⁰⁰

Dash *et al.* selected TiO₂/Co/Al ferromagnetic tunnel contacts and the Schottky barrier was lowered below 50 mV for both electrons and holes.¹¹ The reduction of Schottky barrier is attributed to modulation of band alignment of Co and BP with the application of gate voltage. With the ferromagnetic tunnel contacts, BP FETs exhibit high mobility and large on-state current for hole conduction regime. The hole mobility of 155 cm² V⁻¹ s⁻¹ was achieved while the value for electron was very low (0.18 cm² V⁻¹ s⁻¹), which was the intrinsic characteristic of BP as BP has the lower effective hole mass and higher density of states on the hole side. Moreover, the variation in magnetoresistance tuned by gate voltage was detected, which is also the evidence of modulating the contact resistance and carrier density.

In addition to mobility, the conduction type can be modified by selecting proper metal electrodes. Ye *et al.* tested BP transistors with two contact metals Ni and Pd respectively.⁷⁸ After scaling down the channel lengths to deep submicrometer, transistors with Ni contacts can be tuned from original p-type behaviour to pronounced n-type (as shown in Fig. 6b), which is directly attributed to the reduced Fermi-level pinning at the metal/BP interface. Similar to Cs₂CO₃ modification as mentioned above, owing to the fact that the work function of Ni (5.0 eV) is lower than that of Pd (5.4 eV), an effective Schottky barrier height is reduced resulting from the fact that the Ni metal Fermi-level is closer to the conduction band. This phenomenon is also found in MoS₂ monolayer, in which the metals with a low work function facilitate efficiently electrons injection into the conduction.¹⁰¹ Interestingly, transistors with Pd contacts show smaller contact resistance and superior on-state current and mobility in spite of the higher work function (Fig. 6). They also demonstrated that switching

transport conduction can be implemented by controlling the channel length, back gate voltages, and drain biases.⁷⁸

Moreover, when the Fermi level of the metal contacts is closer to the valence band than the conduction band,^{81,88} further enhancement of current in hole-doped regime can be fulfilled, indicating that selecting proper metal electrodes enables modulating the electrical conduction.

3.1.3 Avoiding surface degradation

Despite the successful preparation of BP flake by mechanical exfoliation, it is inevitable that O₂ and H₂O in ambient exposure irreversibly reacts with BP to form phosphoric acid or oxidized phosphorous compounds and this rapid surface oxidation takes place over a short period of time.^{33,92} The exfoliated surface becomes rough after 1 h⁹² and it becomes obvious when the exfoliated BP crystals are exposed for 24 h.⁹⁰ This surface degradation not only increases the surface roughness but also results in the formation of chemisorbed species, which has several adverse effects including physical changes such as volume expansion and cleated surface, chemical changes towards a liquid phase degrading mobility as well as large Schottky barrier heights due to the metal-induced gap states.^{23, 102, 103} Meanwhile, the oxygen defects (e.g. dangling oxygen) were considered as another reason for surface degradation because oxygen defects are low energy metastable forms which introduce deep donor and/or acceptor levels in the band gap and the dangling oxygen atom can be a starting point for forming more complex defects.¹⁰⁴ The device performances were also influenced significantly by surface degradation. For example, Hersam *et al.* reported that exposure of unencapsulated BP FET in ambient atmosphere induced increasing in threshold voltage, decreased on/off ratio and mobility due to the p-type doping from ambient adsorbates,⁹² in which the charge transfer to trap sites or surface oxidation layer may be the reason for observing large hysteresis in the V_{bg} - I_{ds} curve.^{65,78}

In order to manage this undesired phenomenon, two effective ways were adopted including passivation and solvent exfoliation. The first approach is to deposit AlO_x encapsulation layers acting as barriers against moisture adsorption by atomic layer deposition (ALD) to slow down surface degradation,^{92, 93, 105, 106} and the effects of AlO_x layers on properties are shown in Fig. 7. The on/off ratio of unencapsulated device degraded rapidly upon ambient exposure while AlO_x encapsulated device shows on/off ratio maintaining between 180 and 300 after 175 h. Because of encapsulating and passivating both edge and top surface equivalently by the ALD-derived AlO_x, high on/off ratio of $\sim 3 \times 10^3$ and mobility of $\sim 53 \text{ cm}^2 \text{ V}^{-1} \text{ s}^{-1}$ were maintained even for over 2 weeks in

ambient conditions.⁹² Meanwhile, the positive fixed charges originating from lower ALD growth temperature induced a band bending, changing the polarity of transistor from p-type to ambipolar.⁹³

Lai and Akinwande *et al.* systemically investigated the degradation process of BP transistors with thin and thick Al₂O₃ capping layer over a period of one week by atomic force microscopy (AFM)-based microwave impedance microscope (MIM).¹⁰² The observed change in local resistance indicated that the degradation mostly influences the electronic rather than structural properties. A negative shift of I_d - V_g curves and an increasingly severe hysteresis were observed, suggesting that Al₂O₃ may not be able to provide long-term protection. They further developed a double-layer superstrate by coating fluoropolymer film, which shows strong hydrophobicity and results in the most air-stable device. In addition to Al₂O₃, an encapsulating copolymer capping has been recently reported to effectively suppressed oxidation and the device showed excellent performances: field effect mobility (μ_{FE}) of 600 cm² V⁻¹ s⁻¹ and on/off ratios of 10⁵.⁹⁴

Another way to avoid surface degradation reported recently was by direct liquid exfoliation in anhydrous and oxygen-free organic solvents.^{86, 89, 107-109} As the solvation shell can act as a barrier to prevent oxidative species reaching the nanosheet surface, the oxidation could be effectively minimised by this exfoliation method.¹⁰⁷ For example, Hersam *et al.* found that *N*-methylpyrrolidone (NMP) provides stable and highly concentrated BP dispersions, and the residual NMP leads to reducing the ambient degradation kinetics.⁸⁹ The solvent-exfoliated BP nanosheets transistors show comparable performances such as I_{on}/I_{off} ratio of $\sim 10^4$ and mobility of ~ 50 cm² V⁻¹ s⁻¹, demonstrating that the solution processing is a promising way for fabrication of large-area and high-performance BP devices. Very recently, aprotic and polar solvents such as dimethylformamide (DMF) and dimethyl sulf-oxide (DMSO) were also confirmed as the appropriate solvents for preparing BP flakes, and the liquid-exfoliated sample exhibited competitive electrical properties to mechanically exfoliated counterpart.¹⁰⁹

Özyilmaz *et al.* fabricated black phosphorus passivated in an inert gas environment without chemical precursors or exposure to water.¹¹⁰ No significant roughness change was detected after covering graphene or h-BN and no reaction between BP and passivating crystal was confirmed by Raman spectra. Compared with non-passivated BP devices in which the low electron conduction is attributed to oxygen trap states induced by surface oxidation, partly passivated transistors exhibit enhanced electron transport and improved ambipolar charge transport.

In addition, annealing was found to be an effective approach to managing the surface degradation as it could successfully eliminate the adsorbates on BP surfaces which work as trapping centres for electrons.⁹⁵

3.2 Electric-double-layer transistors

As mentioned before, the decreased mobility of BP transistor is attributed to the unstable surface and the existence of Schottky barrier. In addition to surface passivation, employing high- k materials as the gate dielectrics is also an effective approach to improving mobility.¹¹¹ With higher capacitance, high- k materials can effectively solve the problem of dielectric breakdown and increase the accumulated carrier density. Moreover, electric double layer (EDL) derived from supercapacitors are recently introduced into the transistor to achieve very low voltage operation. With introducing the electrolytes such as polymer electrolytes and ionic liquids/gels, more carriers could be accumulated at the channel/electrolyte interface by applying external electric field and a new kind of transistor named electric double layer transistor (EDLT) is designed for examining the charge transport.^{112, 113}

As the high-density charge carriers can be accumulated by the EDLT technique (e.g. 2DEG over 1×10^{14}), it is possible to explore and investigate some physical mechanisms in 2D semiconductors. For example, the metal-insulator transition predicted theoretically due to the in-layer strain or changing the number of layers in BP³⁷ now has been achieved by using ionic-liquid (IL) gating.⁹⁵ With the application of ionic liquid, the metallic state was achieved and saturation of resistance for both hole and electron channel was observed, as shown in Fig. 8a. Unfortunately, superconductivity was not further detected and there was still an increase of resistance even under the highest gate voltage, which is attributed to the insufficient electron density and predicted that superconductivity might be restricted only in monolayer BP. They further proposed the ambipolar charge accumulation associated with the 2D-3D crossover, and this 3D-like localization behaviour was the result of contribution from hole carriers, as shown in Fig. 8b.

Ionic liquid gating is also beneficial to achieving outstanding device performances and tight gate control. For example, a dual-gate BP transistor with bottom gate SiO₂ and top gate IL dielectric has been recently reported, and the effective oxide thickness (EOT) of ~ 1.5 nm was achieved without gate leakage.⁹⁶ In addition to the superior performances such as transconductance of ~ 240 $\mu\text{S}/\mu\text{m}$ and record high ON current of ~ 200 $\mu\text{A}/\mu\text{m}$, notably, the SS of 65 mV/decade was obtained, which is very close to the limit value of traditional transistors.¹¹⁴ Based on this IL-gated BP transistor, a signal amplifier was fabricated with a gain of ~ 9 and it kept almost unchanged for input signal frequencies up to 15 kHz.

4. BP based Heterostructures

In recent years, building vertical heterostructures based on 2D van der Waals materials has been considered as a creative way to integrate the properties of each isolated components into one system.¹¹⁵ Meanwhile, the

important behaviour of 2D van der Waals heterostructures is that the properties of each component can be conserved in this double-layer or sandwich configuration. Compared with 3D materials, in which crystalline layers are usually bonded tightly to the neighbouring layer, no strain exists in stacked 2D materials because it is unnecessary to form tight bonds within the layers. The only requirement of forming heterostructure is that the layer-by-layer assembly will be achieved only when applying two or more different materials without dangling bonds.¹¹⁶ There are two advantages of using black phosphorus: (i) BP's layered structure resembles other 2D layered structure materials; (ii) and no lattice mismatch between the materials because of the strong van der Waals interaction.¹¹⁷ Therefore, it is expected that the combination of BP with other 2D layered semiconductors or insulators to form heterostructure is promising for transistor applications.

4.1 BP–TMDs

The first BP heterostructure was fabricated to form p-n diode with MoS₂, as shown in Fig. 9a.⁸² As mentioned above, BP exhibits hole-transport-dominated behaviour while MoS₂ is an n-type semiconductor. Therefore, it is anticipated to fabricate an electrically tunable p-n junction based on BP/MoS₂ heterostructure. Strong gate-tunable current-rectifying characteristics indicate that the heterostructure with good ohmic contact between BP and MoS₂ was obtained. Fig. 9b and c show the gate-tunable photoresponse to incident laser, the maximum fill factor ($FF = P_d/I_{sc}V_{oc}$) the peak external quantum efficiency (EQE) were ~0.5 and 0.3% respectively, which is the first report of efficient photovoltaic energy conversion in black phosphorus. The maximum responsivity of 418 mA/W was almost 100 times higher than that of previous BP phototransistor, and superior performances made BP p-n diode as a promising candidate for broad-band photodetection and solar energy harvesting devices. Very recently, another application, Esaki tunnel diode using van de Waals heterojunction composed of BP and SnSe₂ has been fabricated with broken-gap energy band offset for the first time.¹¹⁸

In addition, BP is also an important component for TMD-based heterostructure. For example, after forming artificial heterostacks with few-layer BP, both MoS₂ and WS₂ show significant photoluminescence (PL) quenching, which is attributed to the splitting excitons by the build-in electric fields in the heterostructures.¹¹⁹

4.2 BP–graphene

Since BP and graphene have anisotropic and isotropic structures respectively, it is expected that the anisotropy of black phosphorus could 'leak' into neighbouring layers and induce new characteristics and phenomena on graphene after stacking heterostructures.⁴¹ Padilha *et al.* studied the structural and electronic properties of single-layer and bilayer phosphorene stacked on the top of graphene by density functional

theory.¹¹⁶ In this heterostructure, the electronic structure of both the phosphorene and the graphene layers are almost preserved, indicating that the properties of each component can be conserved. A p-type channel is created as the electrons transferring from the noncontacted phosphorene region to the phosphorene and graphene takes place when the difference between Fermi levels is above zero. Meanwhile, by applying an external electrical field perpendicular to the device, electron transferring also can be induced, which allows modulation of the Schottky barrier height and the doping of phosphorene. In addition, graphene/phosphorene heterostructure has tunable Schottky barrier, which is sensitive to varying the interfacial distance.¹²⁰

A recent article reported that barrier-free contacts were achieved by using graphene with a tunable work-function as source-drain electrodes and h-BN as the encapsulating layer,¹⁰³ as shown in Fig. 10a. The nearly temperature insensitivity of I_{SD} (Fig. 10b) in this graphene-contacted transistor suggests that charge injection is ohmic rather than thermionic emission. However, due to wide gap in bilayer BP, the linear relation is only observed in p-type region and it is insufficient to achieve a perfect band matching by tuning of the Fermi level of graphene with V_{BG} .

4.3 BP-h-BN

h-BN is a wide bandgap insulator with atomically flat surface and it can be used as a gate dielectric material because of its disorder-free interface with other 2D materials.¹²¹ Based on these points, a few-layer black phosphorus PN junctions has been fabricated by using h-BN as gate insulator, and the photogenerated carriers were separated by internal electric field at the PN junction, resulting a photocurrent at zero external bias.⁸¹ The gate-induced stress reported in the previous work was effectively reduced by gating with h-BN flake. After applying opposite local gate bias, the photocurrent and photovoltage are generated, and thus the mechanism is photovoltaic effect originating from the formation of a PN or NP junction, as shown in Fig. 11. Meanwhile, the maximum electrical power P_{ei} of 13 pW and the photovoltaic effect still can be measured under the 940 nm illumination, indicating that the bandgap of the BP flake is smaller than 1.31 eV and the energy harvesting is in near-infrared part of the spectrum.

From the above part, nearly identical output characteristics under both ambient and vacuum conditions were observed after depositing h-BN encapsulating layer (Fig. 10c), suggesting that the high-quality h-BN can successfully protect the BP surface from interaction with air.¹⁰³

To further improve the performances, a sandwich h-BN/BP/h-BN heterostructure, in which the h-BN acts not only as the gate insulator but also as the encapsulation layer to prevent the surface degradation,^{97, 98, 122} has

been designed recently. In Lau's work, such encapsulated devices were comparably stable after more than 300 h under ambient conditions.⁹⁷ The hole mobility was $400 \text{ cm}^2 \text{ V}^{-1} \text{ s}^{-1}$ at room temperature and jumped to $\sim 4,000 \text{ cm}^2 \text{ V}^{-1} \text{ s}^{-1}$ at low temperature region, followed by observed metal-insulator transition. Moreover, Shubnikov de Haas (SdH) oscillations at the magnetic field were observed successively in this series of investigations. For example, Zeeman splitting with an estimated g -factor of ~ 2 was established by SdH oscillations in the magnetic field, which determined the cyclotron mass of charge carriers.⁹⁷ Meanwhile, both quantum oscillations and zero Berry phase were observed in BP hole gas in Wang's study.⁹⁸ These heterostructures between phosphorene and other 2D materials open the door for exploring the quantum oscillations which cannot be observed in thin phosphorene alone.

Since the charged impurities existed at the BP/h-BN interface and the low temperature mobility was limited by impurity-dominated scattering,⁹⁷ Zhang *et al.* have designed to use h-BN for screening the impurity potential very recently.⁴⁵ In this device, a record-breaking μ_{FE} for holes ($3,900 \text{ cm}^2 \text{ V}^{-1} \text{ s}^{-1}$) and electrons ($1,600 \text{ cm}^2 \text{ V}^{-1} \text{ s}^{-1}$) were achieved at 1.5 K, which resulted in presence of quantum oscillations in the extreme quantum limit.

5. Summary and Outlook

In this article, we discussed the structural and fundamental properties of black phosphorus, and the recent progress as well as remaining challenges in BP based FET applications are reviewed. With layer-controlled bandgap, carrier mobility and ambipolar transport, BP shows great potential in nanoelectronic applications, especially for complementary metal oxide semiconductor circuits. In addition, as a member in the family of van der Waals materials, BP is compatible with other two-dimensional layered materials and these heterostructures have been found to exhibit superior device performances. In the last part, we also offer our outlook for the future research:

(i) Searching for new approaches to avoiding surface degradation as the present way by capping layer on the top cannot completely solve the problem because this method just can reduce the degradation rate. For example, deliberately designing a native oxide to protect the underlying layers is a great idea for protecting the underlying BP layers, and this has been reported very recently.¹²³ The native oxide not only provides a stable passivation layer but also is compatible with additional gate insulators for top-gated configuration.

(ii) For practical applications, fabricating large scale BP two-dimensional (2D) materials for future electronic devices and/or flexible devices will be a direction. Meanwhile, a recent study showed that amorphous BP nanoflake can be fabricated at low temperature and the transistor based on this ultrathin film exhibited superior

properties than conventional elemental amorphous channel materials.¹²⁴ Since the processing condition is beneficial for large-scale fabrication, amorphous BP will further draw scientific attention.

(iii) As the doping level is limited by the breakdown electric field of the SiO₂ gate dielectric,⁹ it is expected that higher drain current modulation can be achieved by applying high-*k* gate insulators or electrolytes with higher capacitance.

(iv) Physical phenomenon, for example the superconductivity induced by electron doping, has been studied theoretically in BP and will be achieved experimentally by using electric double layer technique as more carriers can be accumulated at the interface. In addition, a unique 2D electron gas by EDLT technique will provide opportunity for investigating the 2D quantum limit in monolayer phosphorene.

We believe that the research on BP FET applications will attract significant attention and eventually BP will be utilized in future electronics since they can be not only used in transistors but also for many other functional purposes such as thermoelectronics, optoelectronics and sensors. Progress in this field is expected as this material is showing an important impact on the development of van der Waals materials.

Acknowledgements

This work is funded by the Australian Research Council Project (grant no. FT140100032). One of the authors (H. Du) thanks China Scholarship Council (CSC) for financial support (no. 201406410060) and Mr. Rui Ding for valuable discussion.

References

1. F. Schwierz, *Nat. Nanotechnol.*, 2010, **5**, 487-496.
2. K. Novoselov, A. K. Geim, S. Morozov, D. Jiang, M. Katsnelson, I. Grigorieva, S. Dubonos and A. Firsov, *Nature*, 2005, **438**, 197-200.
3. F. Schwierz, J. Pezoldt and R. Granzner, *Nanoscale*, 2015, **7**, 8261-8283.
4. B. Radisavljevic, A. Radenovic, J. Brivio, V. Giacometti and A. Kis, *Nat. Nanotechnol.*, 2011, **6**, 147-150.
5. D. Liu, Y. Guo, L. Fang and J. Robertson, *Appl. Phys. Lett.*, 2013, **103**, 183113.
6. D. Lembke, S. Bertolazzi and A. Kis, *Acc. Chem. Res.*, 2015, **48**, 100-110.
7. Q. H. Wang, K. Kalantar-Zadeh, A. Kis, J. N. Coleman and M. S. Strano, *Nat. Nanotechnol.*, 2012, **7**, 699-712.
8. H. Schmidt, F. Giustiniano and G. Eda, *Chem. Soc. Rev.*, 2015, DOI: 10.1039/c5cs00275c.

9. L. Li, Y. Yu, G. J. Ye, Q. Ge, X. Ou, H. Wu, D. Feng, X. H. Chen and Y. Zhang, *Nat. Nanotechnol.*, 2014, **9**, 372-377.
10. C. M. Park and H. J. Sohn, *Adv. Mater.*, 2007, **19**, 2465-2468.
11. M. V. Kamalakar, B. Madhushankar, A. Dankert and S. P. Dash, *Small*, 2015, **11**, 2209-2216.
12. C. Dean, A. Young, I. Meric, C. Lee, L. Wang, S. Sorgenfrei, K. Watanabe, T. Taniguchi, P. Kim and K. Shepard, *Nat. Nanotechnol.*, 2010, **5**, 722-726.
13. S. Das, M. Demarteau and A. Roelofs, *ACS Nano*, 2014, **8**, 11730-11738.
14. F. Xia, H. Wang and Y. Jia, *Nat. Commun.*, 2014, **5**, 4458.
15. G. Frey, S. Elani, M. Homyonfer, Y. Feldman and R. Tenne, *Phys. Rev. B*, 1998, **57**, 6666.
16. T. Cao, G. Wang, W. Han, H. Ye, C. Zhu, J. Shi, Q. Niu, P. Tan, E. Wang and B. Liu, *Nat. Commun.*, 2012, **3**, 887.
17. Y. Kubota, K. Watanabe, O. Tsuda and T. Taniguchi, *Science*, 2007, **317**, 932-934.
18. K. Watanabe, T. Taniguchi and H. Kanda, *Nat. Mater.*, 2004, **3**, 404-409.
19. V. Tran, R. Soklaski, Y. Liang and L. Yang, *Phys. Rev. B*, 2014, **89**, 235319.
20. K. I. Bolotin, K. Sikes, Z. Jiang, M. Klima, G. Fudenberg, J. Hone, P. Kim and H. Stormer, *Solid State Commun.*, 2008, **146**, 351-355.
21. S. Kim, A. Konar, W.-S. Hwang, J. H. Lee, J. Lee, J. Yang, C. Jung, H. Kim, J.-B. Yoo and J.-Y. Choi, *Nat. Commun.*, 2012, **3**, 1011.
22. H. Liu, Y. Du, Y. Deng and P. D. Ye, *Chem. Soc. Rev.*, 2015, **44**, 2732-2743.
23. H. Liu, A. T. Neal, Z. Zhu, Z. Luo, X. Xu, D. Tománek and P. D. Ye, *ACS Nano*, 2014, **8**, 4033-4041.
24. A. A. Balandin, S. Ghosh, W. Bao, I. Calizo, D. Teweldebrhan, F. Miao and C. N. Lau, *Nano Lett.*, 2008, **8**, 902-907.
25. R. Yan, J. R. Simpson, S. Bertolazzi, J. Brivio, M. Watson, X. Wu, A. Kis, T. Luo, A. R. Hight Walker and H. G. Xing, *ACS Nano*, 2014, **8**, 986-993.
26. S. Sahoo, A. P. Gaur, M. Ahmadi, M. J.-F. Guinel and R. S. Katiyar, *J. Phys. Chem. C*, 2013, **117**, 9042-9047.
27. I. Jo, M. T. Pettes, J. Kim, K. Watanabe, T. Taniguchi, Z. Yao and L. Shi, *Nano Lett.*, 2013, **13**, 550-554.
28. G. A. Slack, *Phys. Rev.*, 1965, **139**, A507.
29. F. Xia, D. B. Farmer, Y.-m. Lin and P. Avouris, *Nano Lett.*, 2010, **10**, 715-718.

30. M. J. Allen, V. C. Tung and R. B. Kaner, *Chem. Rev.*, 2009, **110**, 132-145.
31. M. Xu, T. Liang, M. Shi and H. Chen, *Chem. Rev.*, 2013, **113**, 3766-3798.
32. P. Bridgman, *J. Am. Chem. Soc.*, 1914, **36**, 1344-1363.
33. S. P. Koenig, R. A. Doganov, H. Schmidt, A. C. Neto and B. Oezylmaz, *Appl. Phys. Lett.*, 2014, **104**, 103106.
34. A. Morita, *Appl. Phys. A*, 1986, **39**, 227-242.
35. S. Appalakondaiah, G. Vaitheeswaran, S. Lebegue, N. E. Christensen and A. Svane, *Phys. Rev. B*, 2012, **86**, 035105.
36. Y. Takao, H. Asahina and A. Morita, *J. Phys. Soc. Jpn.*, 1981, **50**, 3362-3369.
37. J. Guan, Z. Zhu and D. Tománek, *Phys. Rev. Lett.*, 2014, **113**, 046804.
38. Z. Zhu and D. Tománek, *Phys. Rev. Lett.*, 2014, **112**, 176802.
39. M. Wu, H. Fu, L. Zhou, K.-L. Yao and X. C. Zeng, *Nano Lett.*, 2015, **15**, 3557-3562.
40. K.-T. Lam, Z. Dong and J. Guo, *IEEE Electron Device Lett.*, 2014, **35**, 963-965.
41. H. O. Churchill and P. Jarillo-Herrero, *Nat. Nanotechnol.*, 2014, **9**, 330-331.
42. D. Shao, W. Lu, H. Lv and Y. Sun, *EPL-Europhys. Lett.*, 2014, **108**, 67004.
43. J. Qiao, X. Kong, Z.-X. Hu, F. Yang and W. Ji, *Nat. Commun.*, 2014, **5**, 4475.
44. X. Wang, A. M. Jones, K. L. Seyler, V. Tran, Y. Jia, H. Zhao, H. Wang, L. Yang, X. Xu and F. Xia, *Nat. Nanotechnol.*, 2015, **10**, 517-521.
45. L. Li, F. Yang, G. J. Ye, Z. Zhang, K. Watanabe, T. Taniguchi, Y. Wang, X. H. Chen and Y. Zhang, *Nat. Nanotechnol.*, 2015, **10**, 608-613.
46. S. Das, W. Zhang, M. Demarteau, A. Hoffmann, M. Dubey and A. Roelofs, *Nano Lett.*, 2014, **14**, 5733-5739.
47. Y. Cai, G. Zhang and Y.-W. Zhang, *Sci. Rep.*, 2014, **4**, 6677.
48. A. Rodin, A. Carvalho and A. C. Neto, *Phys. Rev. Lett.*, 2014, **112**, 176801.
49. A. Manjanath, A. Samanta, T. Pandey and A. K. Singh, *Nanotechnology*, 2015, **26**, 075701.
50. Y. Ge, W. Wan, F. Yang and Y. Yao, *New J. Phys.*, 2015, **17**, 035008.
51. R. Roldán, A. Castellanos-Gomez, E. Cappelluti and F. Guinea, *arXiv preprint arXiv:1504.07926*, 2015.
52. L. Wang, A. Kutana, X. Zou and B. I. Yakobson, *Nanoscale*, 2015, **7**, 9746-9751.
53. A. A. Balandin and D. L. Nika, *Mater. Today*, 2012, **15**, 266-275.

54. L. Zhu, G. Zhang and B. Li, *Phys. Rev. B*, 2014, **90**, 214302.
55. A. Jain and A. J. McGaughey, *Sci. Rep.*, 2015, **5**, 8501.
56. G. Qin, Q.-B. Yan, Z. Qin, S.-Y. Yue, M. Hu and G. Su, *Phys. Chem. Chem. Phys.*, 2015, **17**, 4854-4858.
57. Z. Luo, J. Maassen, Y. Deng, Y. Du, M. S. Lundstrom, P. D. Ye and X. Xu, *arXiv preprint arXiv:1503.06167*, 2015.
58. Z.-Y. Ong, Y. Cai, G. Zhang and Y.-W. Zhang, *J. Phys. Chem. C*, 2014, **118**, 25272-25277.
59. Y. Cai, Q. Ke, G. Zhang, Y. P. Feng, V. B. Shenoy and Y. W. Zhang, *Adv. Funct. Mater.*, 2015, **25**, 2230-2236.
60. J.-W. Jiang, *Nanotechnology*, 2015, **26**, 055701.
61. R. Fei, A. Faghaninia, R. Soklaski, J.-A. Yan, C. Lo and L. Yang, *Nano Lett.*, 2014, **14**, 6393-6399.
62. H. Lv, W. Lu, D. Shao and Y. Sun, *arXiv preprint arXiv:1404.5171*, 2014.
63. J. Zhang, H. Liu, L. Cheng, J. Wei, J. Liang, D. Fan, J. Shi, X. Tang and Q. Zhang, *Sci. Rep.*, 2014, **4**, 6452.
64. G. Qin, Q.-B. Yan, Z. Qin, S.-Y. Yue, H.-J. Cui, Q.-R. Zheng and G. Su, *Sci. Rep.*, 2014, **4**, 6946.
65. T. Hong, B. Chamlagain, W. Lin, H.-J. Chuang, M. Pan, Z. Zhou and Y.-Q. Xu, *Nanoscale*, 2014, **6**, 8978-8983.
66. T. Low, M. Engel, M. Steiner and P. Avouris, *Phys. Rev. B*, 2014, **90**, 081408.
67. E. Flores, J. R. Ares, A. Castellanos-Gomez, M. Barawi, I. J. Ferrer and C. Sánchez, *Appl. Phys. Lett.*, 2015, **106**, 022102.
68. J.-W. Jiang, B.-S. Wang and H. S. Park, *arXiv preprint arXiv:1412.7587*, 2014.
69. X. Ling, L. Liang, S. Huang, A. A. Puzos, D. B. Geohegan, B. G. Sumpter, J. Kong, V. Meunier and M. S. Dresselhaus, *Nano Lett.*, 2015, **15**, 4080-4088.
70. X. Luo, X. Lu, G. K. W. Koon, A. H. Castro Neto, B. Özyilmaz, Q. Xiong and S. Y. Quek, *Nano Lett.*, 2015, **15**, 3931-3938.
71. R. Fei and L. Yang, *Nano Lett.*, 2014, **14**, 2884-2889.
72. X. Peng, Q. Wei and A. Copple, *Phys. Rev. B*, 2014, **90**, 085402.
73. Q. Wei and X. Peng, *Appl. Phys. Lett.*, 2014, **104**, 251915.
74. J.-W. Jiang and H. S. Park, *Nat. Commun.*, 2014, **5**, 4727.
75. J.-W. Jiang and H. S. Park, *J. Phys. D: Appl. Phys.*, 2014, **47**, 385304.

76. Z. Wang, H. Jia, X. Zheng, R. Yang, Z. Wang, G. Ye, X. Chen, J. Shan and P. X.-L. Feng, *Nanoscale*, 2015, **7**, 877-884.
77. W. Zhu, M. N. Yogeesh, S. Yang, S. H. Aldave, J. Kim, S. S. Sonde, L. Tao, N. Lu and D. Akinwande, *Nano Lett.*, 2015, **15**, 1883-1890.
78. Y. Du, H. Liu, Y. Deng and P. D. Ye, *ACS Nano*, 2014, **8**, 10035-10042.
79. F. Liu, Y. Wang, X. Liu, J. Wang and H. Guo, *IEEE Trans. Electron Devices*, 2014, **61**, 3871-3876.
80. M. Buscema, D. J. Groenendijk, S. I. Blanter, G. A. Steele, H. S. van der Zant and A. Castellanos-Gomez, *Nano Lett.*, 2014, **14**, 3347-3352.
81. M. Buscema, D. J. Groenendijk, G. A. Steele, H. S. van der Zant and A. Castellanos-Gomez, *Nat. Commun.*, 2014, **5**, 4651.
82. Y. Deng, Z. Luo, N. J. Conrad, H. Liu, Y. Gong, S. Najmaei, P. M. Ajayan, J. Lou, X. Xu and P. D. Ye, *ACS Nano*, 2014, **8**, 8292-8299.
83. R. Wan, X. Cao and J. Guo, *Appl. Phys. Lett.*, 2014, **105**, 163511.
84. X. Cao and J. Guo, *IEEE Trans. Electron Devices*, 2015, **62**, 659-665.
85. H. Wang, X. Wang, F. Xia, L. Wang, H. Jiang, Q. Xia, M. L. Chin, M. Dubey and S. Han, *Nano Lett.*, 2014, **14**, 6424-6429.
86. S. Lu, L. Miao, Z. Guo, X. Qi, C. Zhao, H. Zhang, S. Wen, D. Tang and D. Fan, *Opt. Express*, 2015, **23**, 11183-11194.
87. N. Youngblood, C. Chen, S. J. Koester and M. Li, *Nat. Photonics*, 2015, **9**, 247-252.
88. D. Xiang, C. Han, J. Wu, S. Zhong, Y. Liu, J. Lin, X.-A. Zhang, W. P. Hu, B. Özyilmaz and A. C. Neto, *Nat. Commun.*, 2015, **6**, 6485.
89. J. Kang, J. D. Wood, S. A. Wells, J.-H. Lee, X. Liu, K.-S. Chen and M. C. Hersam, *ACS Nano*, 2015, **9**, 3596-3604.
90. A. Castellanos-Gomez, L. Vicarelli, E. Prada, J. O. Island, K. Narasimha-Acharya, S. I. Blanter, D. J. Groenendijk, M. Buscema, G. A. Steele and J. Alvarez, *2D Mater.*, 2014, **1**, 025001.
91. N. Haratipour, M. C. Robbins and S. J. Koester, *IEEE Electron Device Lett.*, 2015, **36**, 411-413.
92. J. D. Wood, S. A. Wells, D. Jariwala, K.-S. Chen, E. Cho, V. K. Sangwan, X. Liu, L. J. Lauhon, T. J. Marks and M. C. Hersam, *Nano Lett.*, 2014, **14**, 6964-6970.
93. H. Liu, A. T. Neal, M. Si, Y. Du and P. D. Ye, *IEEE Electron Device Lett.*, 2014, **35**, 795-797.

94. V. Tayari, N. Hemsworth, I. Fakhri, A. Favron, E. Gaufres, G. Gervais, R. Martel and T. Szkopek, *Nat. Commun.*, 2014, **6**, 7702.
95. Y. Saito and Y. Iwasa, *ACS Nano*, 2015, **9**, 3192-3198.
96. S. Das, Z. Wei, L. Thoutam, Z. Xiao, A. Hoffmann, M. Demarteau and A. Roelofs, *IEEE Electron Device Lett.*, 2015, **36**, 621-623.
97. N. Gillgren, D. Wickramaratne, Y. Shi, T. Espiritu, J. Yang, J. Hu, J. Wei, X. Liu, Z. Mao and K. Watanabe, *2D Mater.*, 2015, **2**, 011001.
98. X. Chen, Y. Wu, Z. Wu, S. Xu, L. Wang, Y. Han, W. Ye, T. Han, Y. He, Y. Cai and N. Wang, *Nat. Commun.*, 2015, **6**, 7315.
99. C. Wang, R. Cheng, L. Liao and X. Duan, *Nano Today*, 2013, **8**, 514-530.
100. K. Gong, L. Zhang, W. Ji and H. Guo, *Phys. Rev. B*, 2014, **90**, 125441.
101. I. Popov, G. Seifert and D. Tománek, *Phys. Rev. Lett.*, 2012, **108**, 156802.
102. J.-S. Kim, Y. Liu, W. Zhu, S. Kim, D. Wu, L. Tao, A. Dodabalapur, K. Lai and D. Akinwande, *Sci. Rep.*, 2015, **5**, 8989.
103. A. Avsar, I. J. Vera-Marun, J. Y. Tan, K. Watanabe, T. Taniguchi, A. H. Castro Neto and O. Barbaros, *ACS Nano*, 2015, **9**, 4138-4145.
104. A. Ziletti, A. Carvalho, D. Campbell, D. Coker and A. Neto, *Phys. Rev. Lett.*, 2015, **114**, 046801.
105. X. Luo, Y. Rahbariagh, J. C. Hwang, H. Liu, Y. Du and P. D. Ye, *IEEE Electron Device Lett.*, 2014, **35**, 1314-1316.
106. J. Na, Y. T. Lee, J. A. Lim, D. K. Hwang, G.-T. Kim, W. K. Choi and Y.-W. Song, *ACS Nano*, 2014, **8**, 11753-11762.
107. D. Hanlon, C. Backes, E. Doherty, C. S. Cucinotta, N. C. Berner, C. Boland, K. Lee, P. Lynch, Z. Gholamvand and A. Harvey, *arXiv preprint arXiv:1501.01881*, 2015.
108. J. R. Brent, N. Savjani, E. A. Lewis, S. J. Haigh, D. J. Lewis and P. O'Brien, *Chem. Commun.*, 2014, **50**, 13338-13341.
109. P. Yasaei, B. Kumar, T. Foroozan, C. Wang, M. Asadi, D. Tuschel, J. E. Indacochea, R. F. Klie and A. Salehi-Khojin, *Adv. Mater.*, 2015, **27**, 1887-1892.
110. R. A. Doganov, E. C. O'Farrell, S. P. Koenig, Y. Yeo, A. Ziletti, A. Carvalho, D. K. Campbell, D. F. Coker, K. Watanabe, T. Taniguchi, A. H. C. Neto and B. Özyilmaz, *Nat. Commun.*, 2015, **6**, 6647.
111. D. Jena and A. Konar, *Phys. Rev. Lett.*, 2007, **98**, 136805.

112. S. H. Kim, K. Hong, W. Xie, K. H. Lee, S. Zhang, T. P. Lodge and C. D. Frisbie, *Adv. Mater.*, 2013, **25**, 1822-1846.
113. H. Du, X. Lin, Z. Xu and D. Chu, *J. Mater. Sci.*, 2015, **50**, 5641-5673.
114. V. V. Zhirnov and R. K. Cavin, *Nat. Nanotechnol.*, 2008, **3**, 77-78.
115. A. Geim and I. Grigorieva, *Nature*, 2013, **499**, 419-425.
116. J. Padilha, A. Fazzio and A. J. da Silva, *Phys. Rev. Lett.*, 2015, **114**, 066803.
117. L. Wang, I. Meric, P. Huang, Q. Gao, Y. Gao, H. Tran, T. Taniguchi, K. Watanabe, L. Campos and D. Muller, *Science*, 2013, **342**, 614-617.
118. R. Yan, S. Fathipour, Y. Han, B. Song, S. Xiao, M. Li, N. Ma, V. Protasenko, D. A. Muller and D. Jena, *arXiv preprint arXiv:1504.02810*, 2015.
119. J. Yuan, S. Najmaei, Z. Zhang, J. Zhang, S. Lei, P. M. Ajayan, B. I. Yakobson and J. Lou, *ACS Nano*, 2015, **9**, 555-563.
120. W. Hu and J. Yang, *Comp. Mater. Sci.*, 2015, DOI: 10.1016/j.commatsci.2015.06.033.
121. J. S. Ross, P. Klement, A. M. Jones, N. J. Ghimire, J. Yan, D. Mandrus, T. Taniguchi, K. Watanabe, K. Kitamura and W. Yao, *Nat. Nanotechnol.*, 2014, **9**, 268-272.
122. Y. Cao, A. Mishchenko, G. Yu, K. Khestanova, A. Rooney, E. Prestat, A. Kretinin, P. Blake, M. Shalom and G. Balakrishnan, *Nano Lett.*, 2015, DOI: 10.1021/acs.nanolett.5b00648.
123. M. Edmonds, A. Tadich, A. Carvalho, A. Ziletti, K. O'Donnell, S. Koenig, D. Coker, B. Özyilmaz, A. C. Neto and M. Fuhrer, *ACS Appl. Mater. & Inter.*, 2015, **7**, 14557-14562.
124. Z. Yang, J. Hao, S. Yuan, S. Lin, H. M. Yau, J. Dai and S. P. Lau, *Adv. Mater.*, 2015, **27**, 3748-3754.

Figure captions:

Fig. 1 (a) Atomic structure of multi-layer black phosphorus and (b) monolayer phosphorene.

Fig. 2 Thermal conductivity of BP calculated theoretically by different methods, blue (red) data corresponding to the conductivities along armchair (zigzag) direction. The inset figure shows the anisotropy of thermal conduction. The data are adopted from ref. 54-57.

Fig. 3 (a) Schematic of orthogonal electrical conductance and thermal conductance in monolayer phosphorene. (b, c) Seebeck coefficient according to the doping density under $T = 300$ and 500 K, respectively. (d, e) The thermoelectric figure of merit according to the doping density under $T = 300$ and 500 K, respectively. Reproduced with permission from ref. 61. Copyright 2014, American Chemical Society.

Fig. 4 Configuration of a back-gated black phosphorus field-effect transistor.

Fig. 5 (a) Forward transfer characteristics (V_g from -80 to 80 V) evolution of a BP FET measured at $V_{sd} = 100$ mV in logarithmic scale with increasing Cs_2CO_3 thickness from 0 to 1.5 nm. (b) Linear plot of the transfer curves at 0.5 and 10 nm Cs_2CO_3 coverage with respect to the pristine BP. Inset: schematic illustration of BP device coated by Cs_2CO_3 . (c) UPS spectra evolution at the low kinetic energy region (secondary electron cutoff) with respect to the Cs_2CO_3 thickness. (d) UPS spectra evolution at lower kinetic energy region with increasing MoO_3 coverage. Φ is the work function. Reproduced with permission from ref. 88. Copyright 2015, Nature Publishing Group.

Fig. 6 (a) Contact resistance for both Ni and Pd contact metals at various gate biases in BP transistors. (b) I - V transfer characteristic of Ni contact BP FETs with a channel length from $2 \mu\text{m}$ to 100 nm. (c) I - V transfer characteristic of Pd contact BP FETs with a channel length from $2 \mu\text{m}$ to 100 nm. Reproduced with permission from ref. 78. Copyright 2014, American Chemical Society.

Fig. 7 Time dependence of few-layer BP FET device characteristics. (a) Transfer curves for an unencapsulated BP FET with Ti/Au contacts, measured as a function of ambient exposure time. (b) Transfer curves for a BP FET measured immediately before and after encapsulation. (c) Transfer curves for a ~ 30 nm thick ALD AlO_x encapsulated BP FET with Ti/Au contacts, measured as a function of ambient exposure time. (d) Transfer curves for a ~ 30 nm thick ALD AlO_x encapsulated BP FET with Ni/Au contacts, measured against ambient exposure time. Comparison of the (e) $I_{\text{ON}}/I_{\text{OFF}}$ ratio and (f) hole mobility for encapsulated and unencapsulated Ti/Au BP FETs versus ambient exposure time. Reproduced with permission from ref. 92. Copyright 2014, American Chemical Society.

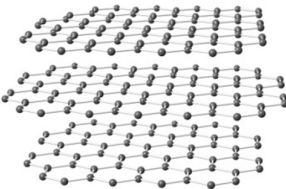
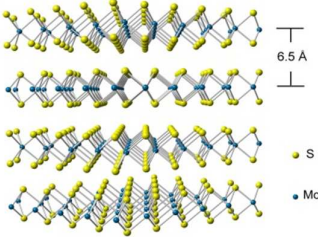
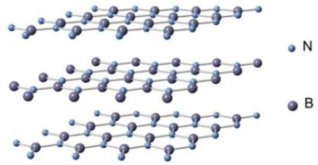
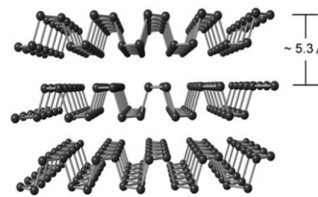
Fig. 8 (a) Temperature dependence of sheet resistance (R_{sheet}) hole transport and electron transport, (b) Temperature dependence of the sheet conductance (σ_{sheet}) for hole transport (left) and electron transport (right) as a function of temperature (T) for different gate voltages (V_{Gate}). Reproduced with permission from ref. 95. Copyright 2015, American Chemical Society.

Fig. 9 (a) Schematics and optical image of the device structure. (b) I - V characteristics of the p-n diode (left) and photocurrent as a function of incident laser power (right). (c) I_d - V_d (left) and power generation as a function of V_d under various laser powers (right). Reproduced with permission from ref. 82. Copyright 2014, American Chemical Society.

Fig. 10 (a) The schematics of the atomically sharp interfaces in encapsulated BP device. (b) Source-drain bias voltage and temperature dependence of bias current of the device utilizing graphene electrodes. (c) Top gate voltage dependence of bias current under vacuum (black line) and ambient conditions (red line). The inset shows the gate voltage dependence of a nonencapsulated device. Reproduced with permission from ref. 103. Copyright 2015, American Chemical Society.

Fig. 11 Photovoltaic effect in a few-layer black phosphorus PN junction. (a) False-colour map of the short-circuit current (I_{sc} , $V_{\text{ds}} = 0$ V) as the voltages on the two local gates are changed independently. (b) False-colour map of the open-circuit voltage (V_{oc} , $I_{\text{ds}} = 0$ A) as the voltages on the two local gates are changed independently. (c) Band diagrams illustrating the photovoltaic mechanism in PN and NP configurations: an impinging photon (red arrow) generates an electron-hole pair that is swept away from the junction region by the built-in electric field. Reproduced with permission from ref. 81. Copyright 2014, Nature Publishing Group.

Table 1 Atomic structures and properties of 2D layered materials

	Graphene	Molybdenum disulfide	Hexagonal boron nitride	Black phosphorus	Ref.
Atomic structure					
Bandgap (eV)	Zero-gap	1.3 (bulk) 1.8 (single layer)	5.97	0.3 – 2	15-19
Mobility (cm ² V ⁻¹ s ⁻¹)	$\sim 2 \times 10^5$	50 – 200 (bulk) 0.1 – 10 (single layer)	–	350 (bulk) 984 (few-layer) 286 (single layer)	4, 9, 20-23
Thermal conductivity (W m ⁻¹ K ⁻¹)	$\sim 5 \times 10^3$	34.5 (monolayer) ~ 52 (few-layer)	360 (11 layers)	12.1	24-28
On/off ratio	100	10^8 (single layer) 10^6 (multilayer)	–	10^5	4, 9, 21, 29
Electrical conduction type	Ambipolar	n-type	–	Ambipolar	30, 31

Materials type

Semimetal

Semiconductor

Insulator

Semiconductor

Table 2 Comparison of thermoelectric properties of BP

Sample	Seebeck coefficient ($\mu\text{V/K}$)	Figure of merit ZT	Power factor ($\mu\text{W cm}^{-1} \text{K}^{-2}$)	Temperature (K)	Theoretically or experimentally	Ref.
Phosphorene	–	~ 1	–	300	Theoretical study	61
Bulk	-114.6	0.22	118.4	300	Theoretical study	62
Phosphorene	198.7	0.30	138.9	300	Theoretical study	62
Bulk	–	0.72	–	800	Theoretical study	64
5-15 nm thick	5–100	–	–	77	Indirect measurement	65
100 nm thick	~ 60	–	–	300	Indirect measurement	66
Bulk	335 to 415	–	–	300–385	Direct measurement	67

Table 3 Summary of characteristics of recent BP transistors

Film Thickness (nm)	Channel Length (μm)	Gate Insulator	Hole Mobility ($\text{cm}^2 \text{V}^{-1} \text{s}^{-1}$)	Electron Mobility ($\text{cm}^2 \text{V}^{-1} \text{s}^{-1}$)	on/off ratio for hole	on/off ratio for electron	Ref.
10	1.6	SiO ₂	984	–	10 ³	–	9
5	1	SiO ₂	286	–	10 ⁴	–	23
–	~ 2	SiO ₂	116	–	10 ⁵	10 ³	46
4.8	–	SiO ₂	214	1	~ 10 ⁴	–	88
5	1	SiO ₂	205	–	> 10 ⁵	–	14
–	–	SiO ₂	300	–	> 10 ³	–	33
–	–	SiO ₂	100	0.5	> 10 ³	10	80
18.7	3	SiO ₂	170.5	–	10 ²	–	78
5	0.69	SiO ₂	155	0.18	10 ⁴	10 ²	11
–	–	SiO ₂	25.9	–	1.6 × 10 ⁴	–	89
~ 15 ^a	–	SiO ₂	~ 200	27	–	–	88
1.6	0.45	SiO ₂	35	12	600	–	90
8.5	0.3	HfO ₂	400	–	2 × 10 ³	–	85
10.7 ± 0.8	0.17	HfO ₂	44	–	1.2 × 10 ³	–	91
11.5	1.5	Al ₂ O ₃ (top)	–	21.9	–	500	87
1.9	2	SiO ₂ (back) / Al ₂ O ₃ (top)	172	38	2.7 × 10 ⁴	4.4 × 10 ³	13
8.9	–	SiO ₂ (back) / Al ₂ O ₃ (top)	49	–	7.5 × 10 ³	–	92
6	0.5	SiO ₂ (back) / Al ₂ O ₃ (top)	95.6	–	10 ⁴	–	93
15	2.7	Polyimide (back) / Al ₂ O ₃ (top)	310	89	10 ³ – 10 ⁴	–	77
5	–	–	180	3	10 ⁴ – 10 ⁵	–	–
~ 47	–	SiO ₂ (back) / PMMA and MMA (top)	600	–	10 ² (180 K)	–	94
20	–	DEME-TFSI	190 (170 K)	20 (170 K)	5 × 10 ³	–	95
~ 5	–	Ionic liquid	510	–	–	–	96
–	–	h-BN	25	0.12	10 ⁴	10 ²	81
–	–	h-BN	400	–	> 10 ⁵	–	97
8	–	h-BN	1350	–	> 10 ⁵	–	98
~ 10	–	h-BN	400	83	–	–	45

DEME-TFSI: *N,N*-diethyl-*N*-(2-methoxyethyl)-*N*-methylammonium bis(trifluoromethyl-sulfonyl)imide; PMMA: polymethyl methacrylate;

MMA: methyl methacrylate; Ionic liquid: 1-butyl-1-methylpyrrolidinium-tris-pentafluoroethyl-trifluorophosphate. ^aThe channel is Cs₂CO₃-modified BP.

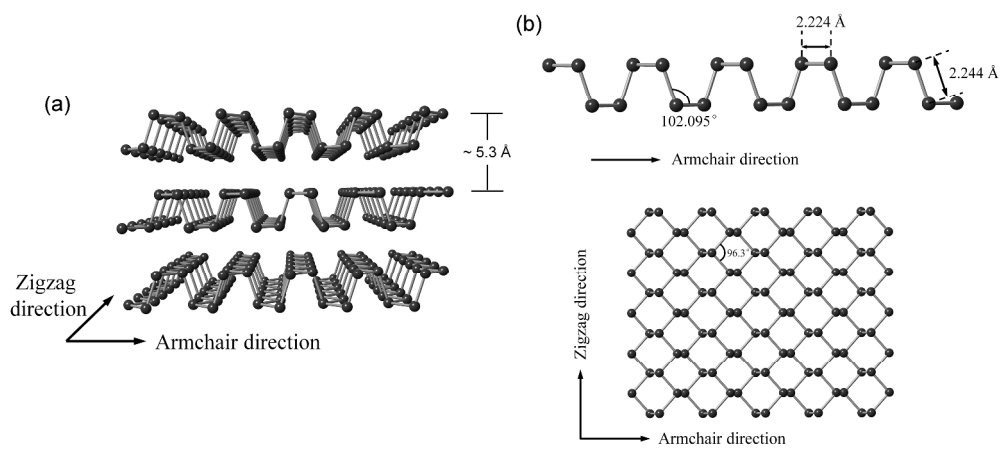


Fig. 1 (a) Atomic structure of multi-layer black phosphorus and (b) monolayer phosphorene
423x187mm (300 x 300 DPI)

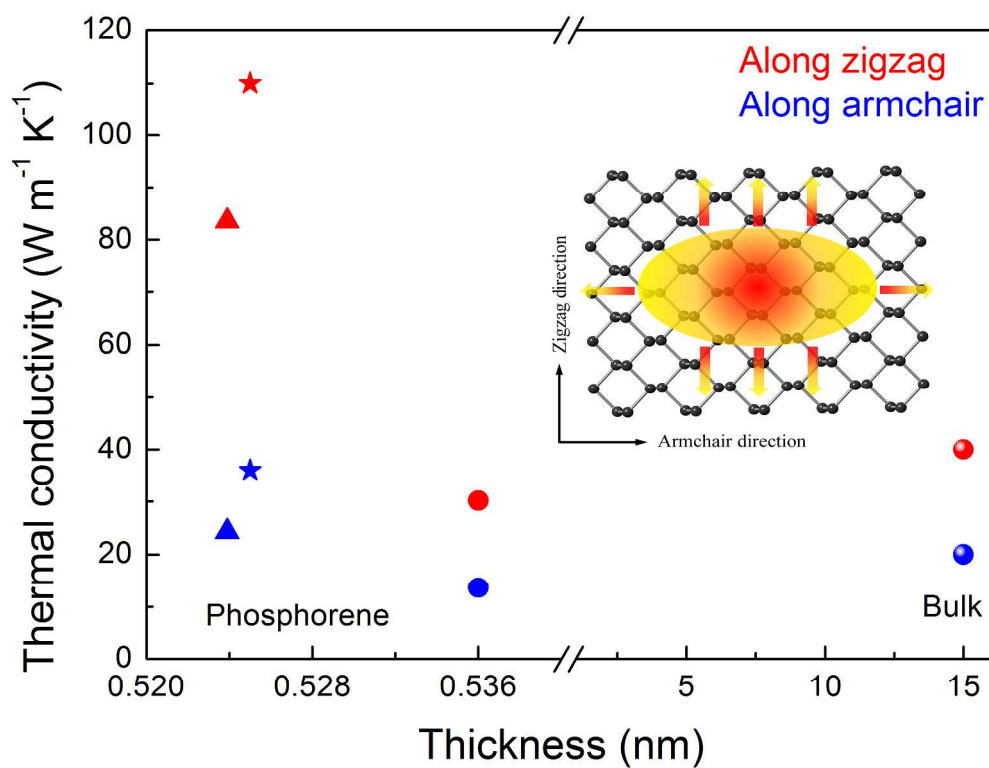


Fig. 2 Thermal conductivity of BP calculated theoretically by different methods, blue (red) data corresponding to the conductivities along armchair (zigzag) direction. The inset figure shows the anisotropy of thermal conduction. The data are adopted from ref. 38-41.
234x182mm (300 x 300 DPI)

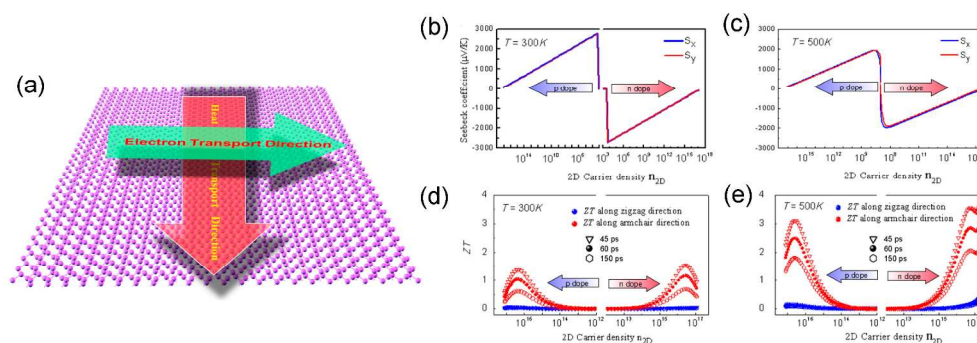


Fig. 3 (a) Schematic of orthogonal electrical conductance and thermal conductance in monolayer phosphorene. (b, c) Seebeck coefficient according to the doping density under $T = 300$ and 500 K, respectively. (d, e) The thermoelectric figure of merit according to the doping density under $T = 300$ and 500 K, respectively. Reproduced with permission from ref. 60. Copyright 2014, American Chemical Society. 302x108mm (300 x 300 DPI)

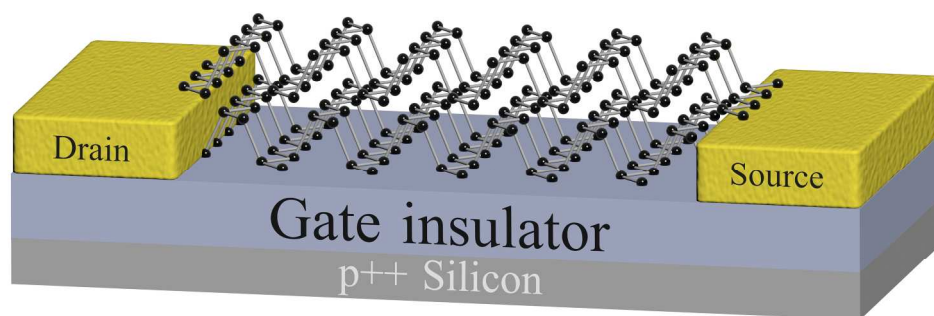


Fig. 4 Configuration of the back-gated black phosphorus field-effect transistor.
338x121mm (300 x 300 DPI)

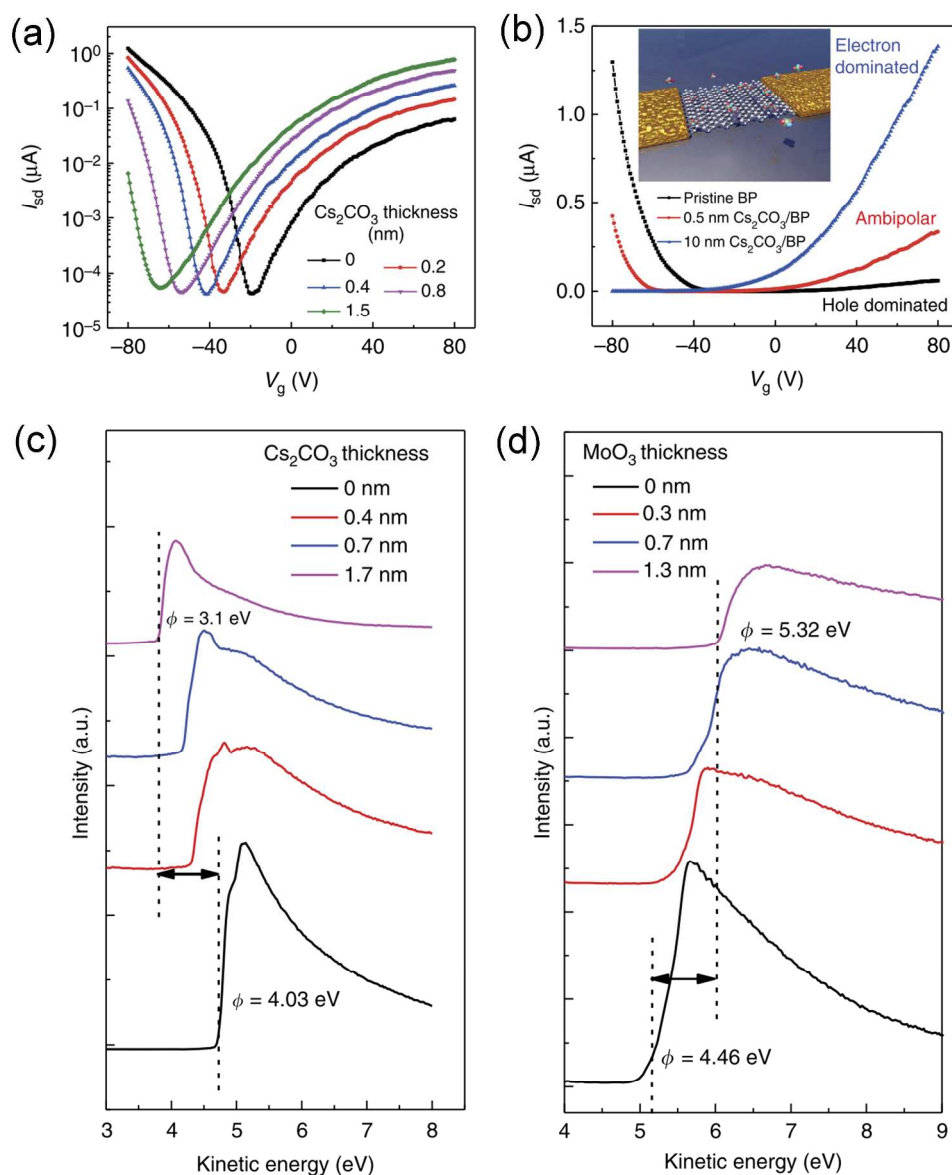


Fig. 5 (a) Forward transfer characteristics (V_g from -80 to 80 V) evolution of a BP FET measured at $V_{sd} = 100$ mV in logarithmic scale with increasing Cs_2CO_3 thickness from 0 to 1.5 nm. (b) Linear plot of the transfer curves at 0.5 and 10 nm Cs_2CO_3 coverage with respect to the pristine BP. Inset: schematic illustration of BP device coated by Cs_2CO_3 . (c) UPS spectra evolution at the low kinetic energy region (secondary electron cutoff) with respect to the Cs_2CO_3 thickness. (d) UPS spectra evolution at lower kinetic energy region with increasing MoO_3 coverage. Φ is the work function. Reproduced with permission from ref. 85. Copyright 2015, Nature Publishing Group.
254x315mm (300 x 300 DPI)

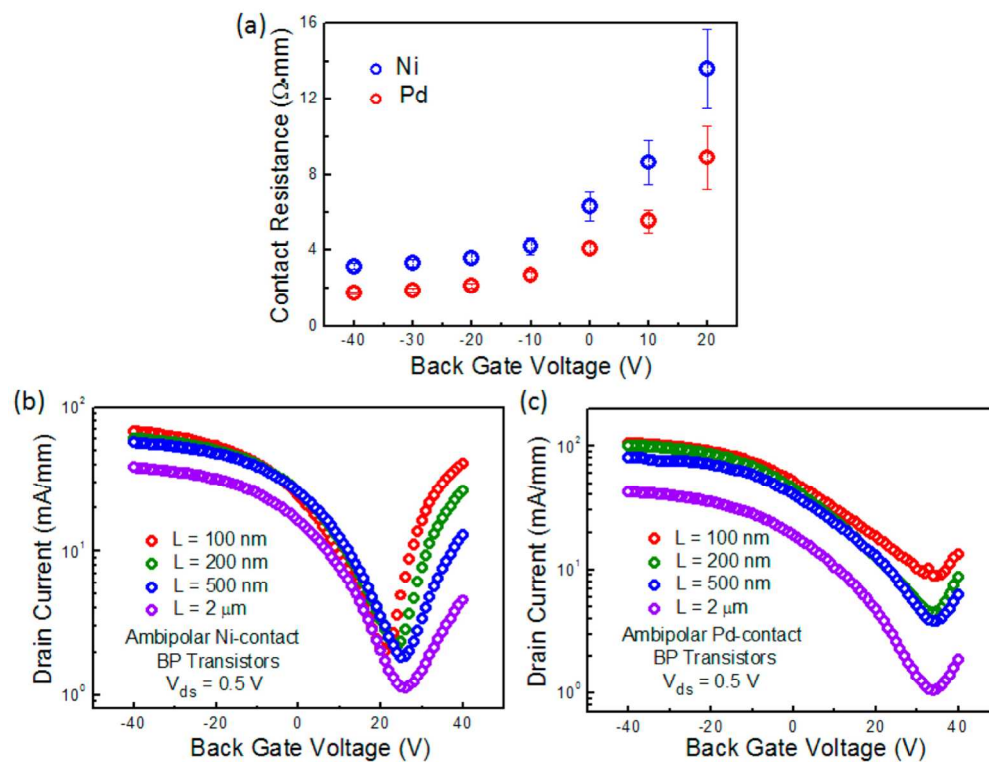


Fig. 6 (a) Contact resistance for both Ni and Pd contact metals at various gate biases. (b) I–V transfer characteristic of Ni contact BP FETs with a channel length from 2 μm to 100 nm. (c) I–V transfer characteristic of Pd contact BP FETs with a channel length from 2 μm to 100 nm. Reproduced with permission from ref. 74. Copyright 2014, American Chemical Society. 136x105mm (300 x 300 DPI)

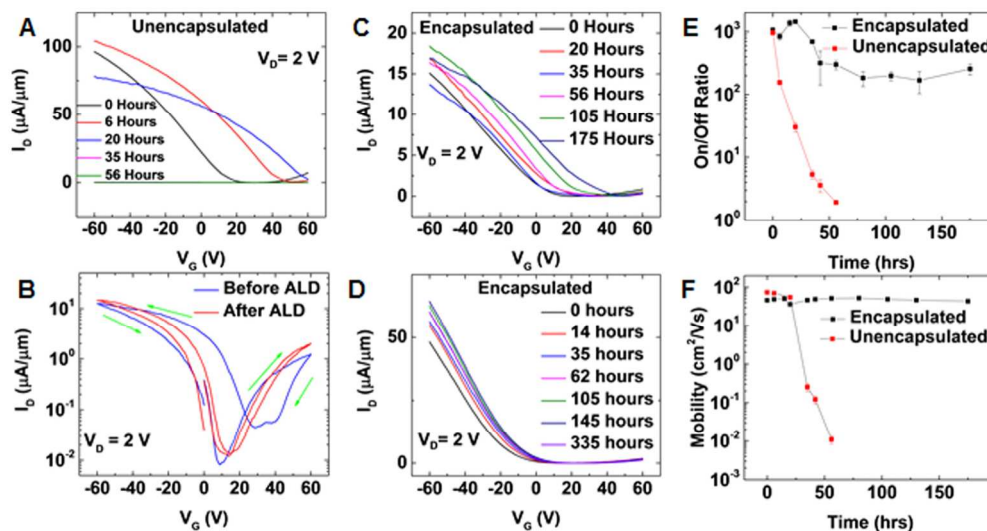


Fig. 7 Time dependence of few-layer BP FET device characteristics. (a) Transfer curves for an unencapsulated BP FET with Ti/Au contacts, measured as a function of ambient exposure time. (b) Transfer curves for a BP FET measured immediately before and after encapsulation. (c) Transfer curves for a ~ 30 nm thick ALD AlOx encapsulated BP FET with Ti/Au contacts, measured as a function of ambient exposure time. (d) Transfer curves for a ~ 30 nm thick ALD AlOx encapsulated BP FET with Ni/Au contacts, measured against ambient exposure time. Comparison of the (e) $I_{\text{ON}}/I_{\text{OFF}}$ ratio and (f) hole mobility for encapsulated and unencapsulated Ti/Au BP FETs versus ambient exposure time. Reproduced with permission from ref. 90.

Copyright 2014, American Chemical Society.

135x72mm (300 x 300 DPI)

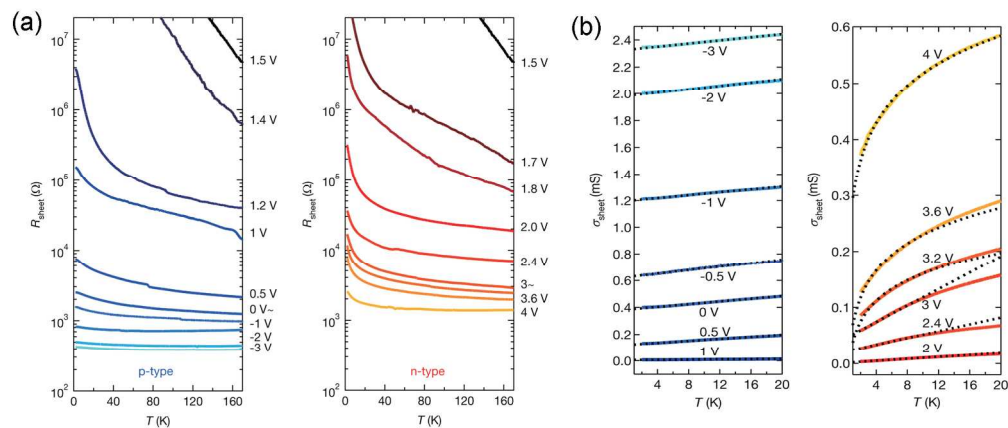


Fig. 8 (a) Temperature dependence of sheet resistance (R_{sheet}) hole transport and electron transport, (b) Temperature dependence of the sheet conductance (σ_{sheet}) for hole transport (left) and electron transport (right) as a function of temperature (T) for different gate voltages (V_{Gate}). Reproduced with permission from ref. 93. Copyright 2015, American Chemical Society. 220x95mm (300 x 300 DPI)

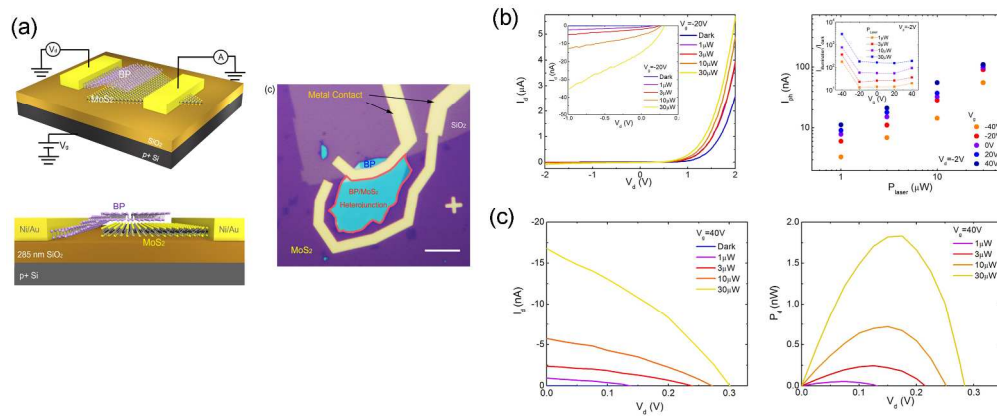


Fig. 9 (a) Schematics and optical image of the device structure. (b) I-V characteristics of the p-n diode (left) and photocurrent as a function of incident laser power (right). (c) I_d - V_d (left) and power generation as a function of V_d under various laser powers (right). Reproduced with permission from ref. 78. Copyright 2014, American Chemical Society. 279x116mm (300 x 300 DPI)

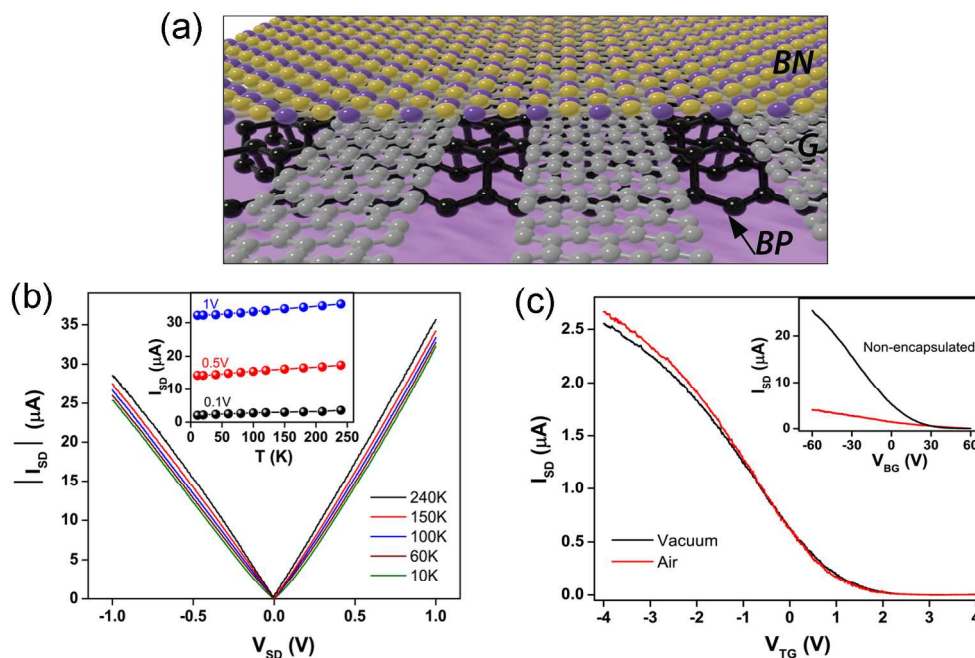


Fig. 10 (a) The schematics of the atomically sharp interfaces in encapsulated BP device. (b) Source-drain bias voltage and temperature dependence of bias current of the device utilizing graphene electrodes. (c) Top gate voltage dependence of bias current under vacuum (black line) and ambient conditions (red line). The inset shows the gate voltage dependence of a nonencapsulated device. Reproduced with permission from ref. 101. Copyright 2015, American Chemical Society.

205x138mm (300 x 300 DPI)

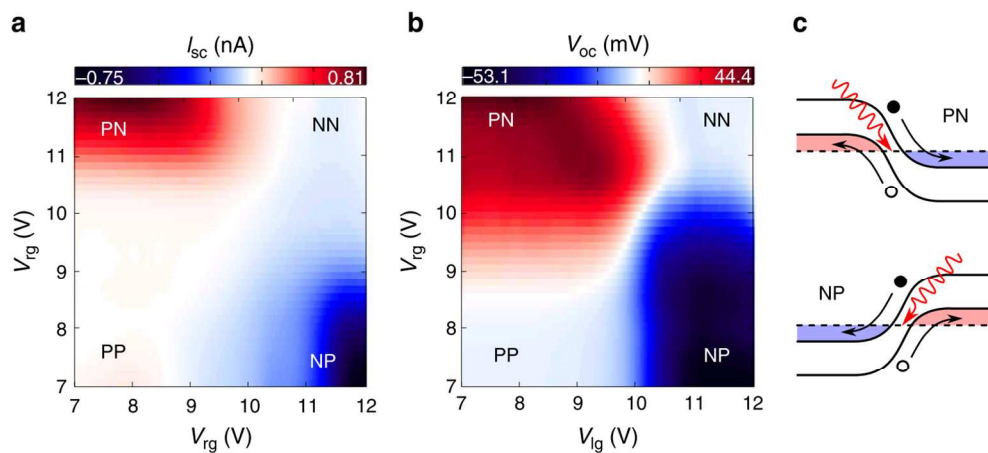


Fig. 11 Photovoltaic effect in a few-layer black phosphorus PN junction. (a) False-colour map of the short-circuit current (I_{sc} , $V_{ds} = 0$ V) as the voltages on the two local gates are changed independently. (b) False-colour map of the open-circuit voltage (V_{oc} , $I_{ds} = 0$ A) as the voltages on the two local gates are changed independently. (c) Band diagrams illustrating the photovoltaic mechanism in PN and NP configurations: an impinging photon (red arrow) generates an electron-hole pair that is swept away from the junction region by the built-in electric field. Reproduced with permission from ref. 77. Copyright 2014, Nature Publishing Group.

129x58mm (300 x 300 DPI)